Corrosion Inspection in High Temperature Surfaces using EMAT Technology

Bernardo Filipe Alves Vicente Farias de Sousa

bernardo.f.sousa@tecnico.ulisboa.pt

Instituto Superior Técnico, Universidade de Lisboa, Portugal

June 2019

Abstract

The present work, developed by *IST* in collaboration with *ISQ*, aimed create a solution to inspect Carbon Steel specimens of thicknesses between 10 mm and 30 mm, for the corrosion mapping of defects of Ø16 mm minimum at critical depths, and thickness discontinuities of 4 mm minimum, in bottom, vertical and bottom-up positions, as well as circular and axial inspections on tubes of Ø 350 mm minimum, between 25ºC and 400ºC, for the Petrochemical Industry. The created prototype, *EMAT Heat Inspection,* consisted of a scanner functioning with an EMAT probe (*Innerspec High Temperature Sensor SH Spiral*) and an encoder (*Hengstler RI32-O/360AR.14KB*) that was air cooled and connected to a dedicated digital device, *Innerspec PowerBox H*, in order to generate corrosion mapping reports. Proper test apparatus and procedures were also created to validate the prototype, studying the amplitude behaviour of back wall and defect signal echoes for different testing blocks regarding desired temperatures. Despite the natural attenuation along increasing temperatures due to scattering effects caused by defect geometries, vibrational interactions between the travelling ultrasonic waves and the microstructures of Carbon Steel, and the different behaviour of cementite vibrational interactions with the ultrasonic waves after reaching its Curie Temperature, the developed prototype fulfilled all the customer requirements, which validated its capacity to inspect, on the given conditions, flaws due to uniform corrosion and erosion corrosion, and defects of critical depth due to pitting corrosion, generating corrosion mapping reports at service temperatures from 25ºC to 400ºC in a practical and reliable manner.

Keywords: EMAT, High Temperature, Corrosion, Attenuation, Non Destructive Testing.

Acronyms

ISQ	Instituto de Soldadura e Qualidade
EMAT	Electromagnetic Acoustic Transducer
UT	Ultrasonic Testing
NDT	Non Destructive Testing
US	United States
SH	Shear Horizontal
AC	Alternating Current
SNR	Signal-to-Noise Ratio
V_T	Shear Wave Velocity [m/s]
E	Young Modulus [N/m^2]
ρ	Density [Kg/m^3]
v	Poisson Ratio
$\vec{B}$	Magnetic Field Density [T]
$\vec{J}$	Current Density [A/m^2]
$\vec{F}_L$	Lorentz Force [N]
A_b	Gain Basis Amplitude [%]
G_b	Gain Basis [dB]
A_o	Origial Amplitude [%]
G_b	Original Gain [dB]

A_e	Edge Echoes Amplitude [%]
A_m	Maximum Echo Amplitude [%]
G	Gain (6 dB Method) [dB]
P_s	Percentual Share [%]
D_O	Obtained Defect Diameter [mm]
D_R	Real Defect Diameter [mm]
SNR_{dB}	Signal to Noise Ratio (in dB) [dB]
A_{AV}	Average of Noise Peaks Amplitude [%]
A_i	Signal Amplitude at Block of Nominal Thickness i [%]
T	Temperature [ºC]

1. Introduction

The annual corrosion costs on the Oil and Gas Industry are estimated to be 1185 billion euros, of which 509 million euros are just for surface pipeline and facility costs, 400 million euros in downhole tubing expenses and 276 million euros in capital expenditures [1]. Surveys account that from 1988 to August 2008, in US, 18% of significant incidents in onshore and offshore pipelines were due to corrosion; in Canadian pipelines, from 2000 to

2006, corrosion ramps up to 50% of the incident causes; and in Europe, from 1970 to 2004, 15% to 17% of the pipeline incidents were also due to corrosion [2]. Corrosion related disasters are prone to result in structural, environmental and human losses, such as the ones that happened in *Shell Oil Co.* Norco refinery (USA, 1988) [3][4], *Silver Eagle* Utah refinery (USA, 2009) [5][6] and *Chevron USA Inc*. Richmond refinery (USA, 2012) [7][8], which were all due to failure of industrial structures due to corrosion effects. In order to effectively mitigate such occurrences, companies could bet in preventive actions, such as the regular conduction of Non Destructive Testing [9]. Also, the increased emphasis on minimizing production costs pulls companies to reduce their plant's maintenance period, and avoiding shutdowns, along with all their inherent high costs [10][11].

For that reason, the present work, developed by *IST,* in collaboration with the *Non Destructive Testing Laboratory* of *ISQ,* aimed to develop an appropriate solution for the increased customer demand to perform corrosion inspections in high temperature Carbon Steel structures. Customers wanted the following criteria to be fulfilled:

- Detect defects with minimum diameter of 16 mm and depth of 50% of the nominal specimen thickness – this is the critical depth, decided by the customer, which determines the replacement of the inspected structure – from 10 mm to 30 mm, up to 400ºC.

- Detect thickness discontinuities of at least 4 mm depth in structures of 10 mm nominal thickness up to 400ºC.

- Perform circumferential and axial inspections on pipes with a minimum outer diameter of 350 m.

- Perform bottom, vertical and upside-down inspections.

- The production site won't need to be shut down in order to perform the testing.

- No more than 10 minutes of setup time.

- Minimum scanning speed of 15 mm/s.

- Generate Corrosion Mapping Reports (A-Scan and C-Scan).

- The inspection equipment must be portable enough to be taken to spaces of difficult access.

It was also known that the causes of most corrosion defects customers wanted to see monitored were uniform corrosion, erosion corrosion and pitting corrosion.

A market survey over various NDT equipments for corrosion inspections on high temperature structures showed there was no offer at that moment which could satisfy the requirement for maximum service temperature of 400ºC:

- *Silverwing RMS2*, which used Conventional UT technology, had a much complex and prolonged setup practice (adjustment of its water pumping system and fitting of the whole equipment on the desired structures), wasting a substantial amount of time. Withal, its intricate software needed a higher level of expertise. And also, it was not suitable for temperatures above 200ºC.

- *Phoenix SSHTC*, which also operated with Conventional UT, was a very rudimental solution. As it is, it couldn't even perform C-Scans for corrosion mapping. And like Silverwing RMS2, it could only operate up to 200ºC.

- *Eddyfi Lyft*, functioning with Eddy Current technology, had a service temperature that was even more restricted than the aforementioned models, reaching 120ºC at best conditions, which made it totally unsuitable for the desired inspections.

Therefore, the practical objective of the present work was to create an appropriate prototype equipment, called *EMAT Heat Inspection*, using the NDT technology of EMATs, as well as creating all the necessary validation apparatus, in order to perform various validation tests on the *EMAT Heat Inspection* prototype which would prove its capability to perform inspections in real Engineering context, thus offering a competitive solution for Inspection Services market on high temperature corrosion mapping of Carbon Steel structures.

1.1. EMAT functioning principle

The functioning principle of EMAT technology at the present work is based on the simultaneous action of two components – the magnetic field generated by a permanent magnet (in some cases, an electromagnet or a pulsed magnet) and the dynamic current which travels through a coil [12][13]. In transmitting mode, it imposes an electromagnetic field on the examined material, creating (by means of two main phenomena, Lorentz Forces and Magnetostriction [14]) an elastic field on its surface and generating ultrasonic waves. The reciprocal is also true in receiving mode - the ultrasonic waves are converted in electrical signals by the transducer [12][15].

In ferromagnetic materials, the presence of the static magnetic field density $\vec{B}$ in the material, created by the magnet, and the Eddy Current density $\vec{J}$, generated by the magnetic field that the AC current passing the coil induces [15], will generate the Lorentz Force $\vec{F_L}$ at the surface region of the inspected material, given by the external product [16]:

$$\vec{F}_L = \vec{B} \times \vec{J} \qquad (1)$$

This body force will mainly create an elastic Transversal, or Shear Horizontal (SH) ultrasonic wave on the material, (perpendicular to $\vec{F}_L$), as the Lorentz Force has a dynamic character along its length, which is conferred by the alternating current passing through the coil [16].

SH waves are also caused by the effect of magnetostriction, which occurs due to the orbital changes in the electrons on the surface region of the inspected material, in order to minimize their energy in the presence of an external magnetic field [12]. The combined effect of the static magnetic field caused by the magnet and the dynamic magnetic field caused by the passing of AC current through the coil modulates the magnetostrictive response along the material – in other words, the material extends and shortens about the length established by the bias field, producing periodic magnetostrictive stresses (that exist in addition to the stresses produced by Lorentz Forces [17]) which disembogue in the propagation of ultrasonic waves [13][15]. In the prototype of the present work, the main functioning mechanism is the Lorentz Force, as depicted in the scheme Fig. 1 (adapted from [12]).
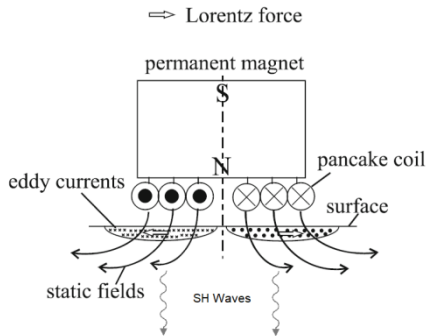

Fig. 1 - General functioning scheme of EMAT technology for the present prototype, with a permanent cylindrical magnet and a pancake coil (adapted from [12]).

The SH wave velocity is given by the following equation [18]:

$$V_T = \sqrt{\frac{E}{\rho} \frac{1}{2(1 + v)}} \qquad (2)$$

The waves travel along the specimen until a discontinuity between mediums of different acoustic impedances is found. Then, ideally, part of the ultrasonic waves is reflected and other is transmitted over the respective interface [19][18][20].

The receiving process behaves in general by the inverse phenomena of Lorentz and Magnetostrictive Forces [15]. The dynamic deformation of a reflected acoustic wave, coupled with the steady magnetic field $\vec{B}$ to which the material is subjected, induces Eddy Currents on the material surface region, inherently creating dynamic electromagnetic fields, which can pass the material surface and be detected by the coil [12][15]. The dynamic electric field induced by the deformation is the reverse Lorentz Force mechanism [12]. Also, the elastic deformation disturbs the magnetization state, resulting in an additional magnetic density flux. This is the piezomagnetic effect, or in other terms, the reversed magnetostriction mechanism [12].

2.1. *EMAT Heat Inspection* prototype

The created prototype, *EMAT Heat Inspection,* consisted of a scanner functioning with an EMAT probe (*Innerspec High Temperature Sensor SH Spiral*) and an encoder (*Hengstler RI32-O/360AR.14KB*) that was air cooled and connected to a dedicated digital device, *Innerspec PowerBox H,* in order to generate corrosion mapping reports.

The probe had a SH Lorentz permanent magnet. SH stands for Shear Horizontal, meaning it was built to perform inspections using Shear Horizontal waves [21], while Lorentz relates to the effect that contributes the most for the generation of ultrasonic waves in this probe, which was the Lorentz Force (as already seen) [22]. It also had a pancake coil, following the same configuration as in scheme of Fig. 1.

The encoder was of the incremental optical rotary type, having maximum rotation speeds of 6000 rpm. It used optical sensing technology that had an embedded rotation code and a pattern, being able to provide signals (in the form of pulses) that could be easily interpreted to provide motion related information such as velocity or change in position [23].

PowerBox H was a dedicated digital equipment, which had the ability to edit various probe settings for optimal inspection performance regarding each specific specimen. It also generated reports in various formats such as A-Scans or C-Scans, delivering real-time display of results.

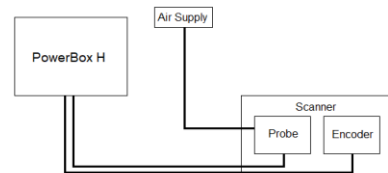A general schematic is presented in Fig. 2:

Fig. 2 - General schematic of *EMAT Heat Inspection* equipment.

As could be noted, the probe and the encoder were not directly connected – they both plugged to the *PowerBox H* device. In order to avoid opening the scanner each time one wanted to connect/disconnect the probe or

the encoder, the most practical solution was to fix three panel connectors to the scanner casing: one for the electrical connection between the encoder and the *PowerBox H*, other for the electrical connection between the probe and the *PowerBox H* and finally another for the air supply to the probe. The probe and encoder were permanently connected to the panel connectors inside the scanner. When the equipment was being used, the *PowerBox H* and the air supply were connected to the panel connectors in the scanner casing, and after usage they were simply disconnected from the panel connectors. The air hose inside the scanner was slightly punctured in order to cool the scanner interior.

After performing anatomical studies to find the most ergonomical design, adequate structures were modelled and produced in order to properly assemble the probe and encoder inside the scanner prototype, which top, handle and base were made of Aluminium, for reduced weight, and the middle casing, as well as the wheels, were made of Stainless Steel for increased structural resistance and durability. The handle was hollow for the air flux of the scanner interior to cool the user's hand. Fig. 3 shows internal views of the final model, designed with *Solidworks 2017* software, and of the created prototype. Fig. 4 shows the created prototype in its travelling case (*Peli 1610*) along with *PowerBox H*, its respective assembly of connection cables (called umbilical cord) and an SD card case.
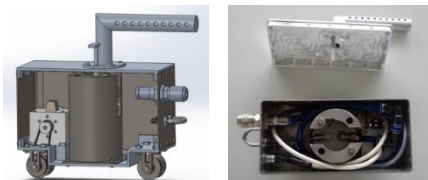

Fig. 3 - Left: prototype final model external view. Right: created prototype internal view.

Fig. 4 - *EMAT Heat Inspection* complete equipment in its travelling case.

2.2. Construction of validation equipment

To perform tests with increased temperatures, a heating box was specially created for the purpose. The case was made by 4 s-shaped bent plates, of Stainless Steel, having a Stainless Steel thick plate as base, and an interior with 10 mm Superwool insulating board on each

wall and on the base (Superwool was a material with very low thermal conductivity and resistant to temperatures up to 900ºC, which was ideal to retain the heat generated inside the box [24]) and four resistors of 5 nuclei each, which had also Ø32 mm, length of 275 mm, 230 V and 1000 W each. They were supported by a Stainless Steel structure, threaded to the base.

The box was designed so that various test blocks with different thicknesses and defects could be easily inserted and removed from the top of the box, being able to lodge up to six blocks of 40 mm width at the same time. The blocks would be heated by the resistors, having a temperature range from 25ºC (room temperature) to 400ºC due to a power regulator. Then, the scanner would be put on top of the blocks, and performed various inspections with *PowerBox H* at increasing temperatures for its results to be validated. A structure made of Aluminium profiles was put on top of the heating box to limitate the starting and ending point, so that these measures would be the same for every inspection made.

The Low Carbon Steel blocks could be divided in three categories:

1st Category - Five blocks for defect detection of different thicknesses: 10 mm, 15 mm, 20 mm, 25 mm and 30 mm. They all had the same length (248 mm) and width (40 mm), and five blind flat bottom holes of Ø12 mm, Ø14 mm, Ø16 mm and Ø18 mm, all having the same disposition. The depths of the holes were the following:

  a. 5 mm for the 10 mm thickness block.
  b. 7,5 mm for the 15 mm thickness block.
  c. 10 mm for the 20 mm thickness block.
  d. 12,5 mm for the 25 mm thickness block.
  e. 15 mm for the 30 mm thickness block.

All the hole depths corresponded to the critical depth for each respective thickness.

2nd Category - One stair block, of 248 mm length and 40 mm width, which had various steps with thicknesses ranging from 30 mm to 12 mm, in 2 mm intervals. This block would allow to verify to what extent the scanner was sensible to thickness variations.

3rd Category - One large block of 10 mm thickness with 248 mm length and 80 mm width, which had three blind flat bottom holes of 2 mm, 3 mm and 4 mm depths and Ø40 mm each. This would permit to study how the scanner was sensible to depth variations at the minimum nominal thickness required.

The distance between defects was enough to guarantee no overlap of detected signals.

In order to check the surface temperature of each block on top of the heating box, a thermometer *Kane May KM 3000* with thermocouple was used.

The four 1000 W resistors inside the heating box granted an even distribution of temperature along the length of each block, with maximum variance of 5 ºC. Fig. 5 shows an inside and outside view of the heating box.

Fig. 5 - Left: various testing blocks on top of the heating box. Right: structure of aluminium profiles on the heating box.

2.3. Prototype Testing Plan

The following tests were proposed for each block category:

1st Category

a. Study of the behaviour of the signal amplitudes related to the nominal thicknesses and defect depths along increasing temperatures, from 25ºC to 400ºC in intervals of 25ºC. That would validate the equipment detectability of critical depths at higher temperatures.

b. Study of the equipment capability for defect dimensioning, comparing the defect diameter results obtained during the tests, with the real flaw diameters, at increasing temperatures from 25ºC to 400ºC, in 25ºC intervals.

c. Study of the signal to noise ratio (SNR) regarding nominal thicknesses and defect depths at increasing temperatures from 25ºC to 400ºC, in 25ºC intervals.

2nd Category

a. Study of the signal amplitudes related to the different thicknesses at increasing temperatures, from 25ºC to 400ºC, in 25ºC intervals, analysing the equipment detectability of back wall thicknesses at increasing temperatures.

b. Study of the signal-to-noise ratio (SNR) regarding different thicknesses at increasing temperatures from 25ºC to 400ºC, in 25ºC intervals.

3rd Category

a. Study of the signal amplitudes related to the nominal thickness and defect depths at increasing temperatures, from 25ºC to 400ºC, in 25ºC intervals, allowing to understand the equipment detectability of different flaw depths at increasing temperatures.

b. Study of the signal-to-noise ratio (SNR) regarding nominal thickness and flaw depths at

increasing temperatures from 25ºC to 400ºC, in 25ºC intervals.

All the tests were recorded in A+C Scans using *PowerBox H*. But not all were performed at the same Gain (which was adjusted to every particular case for better results), therefore, the signal amplitudes needed to be reduced to an equal Gain basis, using the following equation:

$$A_b = \frac{A_o}{10^{\left|\frac{G_o - G_b}{20}\right|}} \qquad (3)$$

The chosen Gain basis G_b, equal for every test performed on the blocks, was 90 dB.

About the study for critical defect dimensioning on the first category blocks, one of the most commonly used methods for flaw sizing was the 6 dB method [25], which consisted in positioning the probe above the flaw until the maximum defect amplitude was found, after which the amplitude of echoes which represented the beginning and ending of the defect were calculated using the following equation:

$$A_e = \frac{A_m}{10^{\left|\frac{G}{20}\right|}} \qquad (4)$$

Where G, the gain drop, was equal to 6 dB. Therefore, it was admitted that a drop of 6 dB over the intensity of the maximum amplitude of the defect echo would give the amplitudes of the echoes between which the defect was present. By using the C-Scan, the block positions, where these echoes are present, could be found, thus giving the flaw dimension [18][26].

Nevertheless, that method was developed to be used in Conventional Ultrasonic Testing. Therefore, experiments with 5 dB, 6 dB and 7 dB have shown that for that particular EMAT probe, using a value of 7 dB in equation (4) instead of 6 dB led to more accurate results.

For each defect diameter, the percentual share, over the real defect diameter, of the difference between the obtained flaw diameter (according to the aforementioned method), and the real flaw diameter, was given by the following formula [26]:

$$P_s = \frac{D_O - D_R}{D_R} \times 100 \qquad (5)$$

For EMAT technology, the adopted SNR equation should be the following [27]:

$$SNR_{dB} = 20log_{10}\left(\frac{A_S}{A_{AV}}\right) \qquad (6)$$

And SNR values below $SNR_{dB} = 20log_{10}(3) = 9,54\ dB$ should be rejected [26].

2.4. Study of Results

For the first category blocks, all A+C Scans were done on the second back wall echoes and second defect echoes, which results were exposed in Amplitude vs. Temperature charts, for each specific point (either a defect of back wall), as seen in the example of Fig. 6 for Ø16 mm defect.
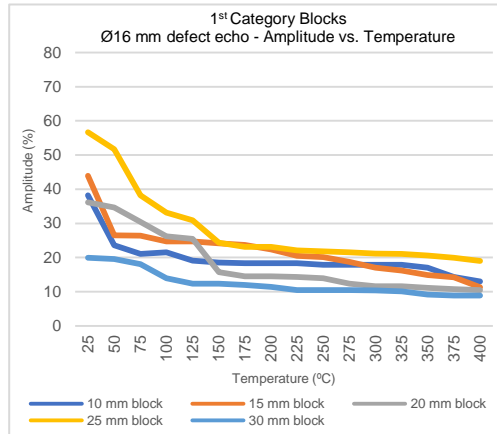

Fig. 6 - Amplitude vs. Temperature for the 1st category blocks Ø16 mm defect echo.

All charts show a descending tendency of their amplitudes along increasing temperatures, which agreed with the findings of Darbari et al. [28], and Papadakis et al. [29]. That phenomenon was known as attenuation, a decrease in the travelling ultrasonic wave intensity when on a certain tested material, due to the main contributions of scattering and absorption [30].

Absorption happens when part of the travelling ultrasonic waves are converted to heat in the material, but usually, its effect is not significant and can be ignored [31].

Scattering could result from the non-homogeneous nature of many polycrystalline materials, which on its grain limits present discontinuities of different acoustic impedances between mediums, due to variations in density, elastic properties or acoustic velocities [18][30]. Thus, when an ultrasonic wave is passing from one grain to another, part of it is scattered on the grain limit [28]. The energy loss due to scattering effect could depend on the frequency and polarization of the ultrasonic waves, the grain size of the material, and also the anisotropy of the material [28]. The frequency used in all the validation tests was 3800 kHz, the value around which gave the best response from the probe when using Shear Horizontal waves, as previously seen, thus minimizing the scattering effect by that source. As it was exposed by Tripathi and Verma, scattering due to the increase of grain size in Carbon Steels is a phenomenon that starts to occur at 900ºC [32], well above the temperature range of the performed tests, therefore it shouldn't be taken in consideration. And finally, Low Carbon Steel is an isotropic material (having identical properties in all directions [33]), so scattering due to anisotropy didn't apply on that case.

Scattering could also be caused by vibrational interactions between the travelling ultrasonic waves and the microstructures of the materials, which (in a general manner) increase with temperature, thus being the major cause of attenuation on the given temperature range, as stated by Lunn et al. [27]. The presence of defects could also promote scattering of the travelling ultrasonic waves due to geometrical discontinuities along the tested specimen [30], and that was clearly the case with first category blocks, which imposed the use of higher Gain values to counteract its effect on amplitude reduction.

Also, most charts showed that amplitude had an accentuated drop from 25ºC to about 200ºC - 225ºC, from which it demonstrated a narrower decrease up to 400ºC. The slight decrease in attenuation tendency when it reached between 200ºC to 225ºC was precisely due to a reduction in microstructural oscillations of cementite (Fe_3C, a typical constituent of Carbon Steels, at temperatures below 727ºC, knowing that Low Carbon Steels usually contain less than 0,25% weight of Carbon [33]), when its respective Curie Temperature (T_c) was reached (around 215ºC) [28][32]. These oscillations enhanced attenuation in a ferromagnetic state but as temperature rose above T_c, cementite became paramagnetic and the oscillations became weaker, therefore attenuation became subtler [28][34].

As it was noted, amplitudes regarding echoes of defects tended to increase with flaw diameters. Smaller defects of Ø12 mm and Ø14 were more difficult to detect. Furthermore, it was also seen that, as defect diameter increased, the amplitude of the defects tended to approach the amplitude of the nominal thickness (and when defect diameters decreased, chart slopes tended to get flatter, hence the increased difficulty to detect smaller defects). Charts also tended to exhibit similar behaviour over the same point (whether it was a defect or back wall).

As an example, the percentual share, over the real defect diameter, of the difference between the obtained flaw diameter (according to the aforementioned method), and the real flaw diameter (as in equation (5)) at the 10 mm block, was exposed on the following Table 1:

Temp.\Defect	Ø12 mm	Ø14 mm	Ø16 mm	Ø18 mm
25 ºC	66,67 %	-21,43 %	-37,50 %	-33,33 %
50 ºC	-41,67 %	-35,71 %	-25 %	-33,33 %
75 ºC	25 %	0 %	-6,25 %	-33,33 %
100 ºC	-25 %	-7,14 %	-43,75 %	-27,78 %
125 ºC	50 %	-28,57 %	-18,75 %	11,11 %
150 ºC	8,33 %	35,71 %	-62,50 %	-11,11 %
175 ºC	-8,33 %	-28,57 %	-25 %	-38,89 %
200 ºC	33,33 %	-28,57 %	-37,50 %	-22,22 %
225 ºC	0 %	-28,57 %	-25 %	-33,33 %
250 ºC	83,33 %	50 %	0 %	-27,78 %
275 ºC	16,67 %	-28,57 %	18,75 %	-27,78 %
300 ºC	0 %	-42,86 %	6,25 %	-33,38 %
325 ºC	-8,33 %	-35,71 %	-12,5 %	-33,33 %
350 ºC	8,33 %	57,14 %	-18,75 %	-22,22 %
375 ºC	-25 %	28,57 %	-31,25 %	27,78 %
400 ºC	-8,33 %	35,71 %	-6,25 %	-33,33 %

Table 1 - Percentual share over the real defect diameter of the difference between obtained and real flaw diameter for 10 mm block of the first category.

The negative values meant the obtained diameter was smaller than the real. And except for a few exceptions where there was no difference (0%), there was great disparity between the obtained results and real dimensions, as most of the percentual differences of defect diameters were well above 20%, reaching in some cases as high as 92,86% of the real defect diameter. Therefore, this equipment was not suitable for defect dimensioning, but that was not a matter of great concern, as what was really important during the kind of inspections that the equipment was designed to perform, was that it could effectively detect defects of critical depth above the required diameter of 16 mm.

Regarding the study of SNR values over temperature, noise amplitudes ranged from 5% to 15% during the tests, being the most common values between 7,5% and 10%. Most chars had a slight descending behaviour, which demonstrated the effect of decreasing amplitudes along higher temperatures. Also, SNR decreased with shorter defect diameters, (which was mainly due to the decrease in signal amplitude in smaller defects), tending to approach the Rejection Value of 9,54 dB. Charts showed that SNR values from Ø12 mm defects were generally very close (or even equal) to the Rejection Value, which means this equipment wasn't fit to detect defects as short as Ø12 mm. SNR values from Ø14 mm defects were not as close as the previous ones, but a mean value of 11 dB was still low, considering the charts for Ø16 mm defects, with values between 13 dB to 16 dB, and for Ø18 mm defects, ranging from 14 dB to 20 dB.

Because, as SNR values successively decreased from Ø18 mm to Ø14 mm and Ø12 mm defects, charts became less sparse and defect amplitudes tended to approximate

noise amplitudes, being increasingly difficult to clearly detect lower diameter defects. Withal, simultaneous analysis of the charts for SNR vs. Temperature and Amplitude vs. Temperature has proven that defects of critical depth from Ø16 mm up could easily and clearly be detected at temperatures from 25ºC to 400ºC, for all given blocks.

For that reason, it was decided to apply a safety margin, declaring that the minimum defect diameter (of critical depth), from 10 mm to 30 mm nominal thickness blocks, which this equipment could clearly detect was Ø16 mm, as required by *ISQ* customers. Fig. 7 shows an example of the SNR vs. Temperature charts for the Ø16 mm defect.
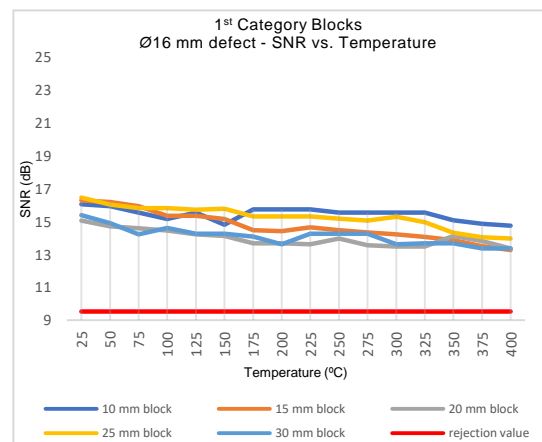

Fig. 7 - SNR vs. Temperature for the 1st category blocks Ø16 mm defect echo, along with the respective rejection value.

Regarding the second category step block, A+C Scan results were properly treated (using a Gain Basis of 90 dB and the same proceedings as with the first category blocks), so that charts regarding back wall echo signal amplitude evolution along increasing temperatures, as well as SNR versus temperature, could be presented.

Charts of the back wall echo amplitude along increasing temperatures for the second category step block showed that amplitudes regarding each step followed the same descending tendency as the back wall echo amplitudes of the first category blocks, generally presenting a slight slope change at 200ºC - 225ºC (near the Curie Temperature of cementite) for the same reasons previously explained with other blocks.

In that case, only back wall echoes were analysed. Then, as there were no defects of critical depth, scattering effects were reduced, allowing the use of lower Gain values to obtain decent amplitude results which, after being reduced to the same Gain basis, led to greater back wall echo amplitudes when compared with the ones of first category blocks. Noise was also reduced by these effects, having a mean value of 5%.

For the SNR versus Temperature study, the same proceedings as the previous blocks were used (Rejection Value of 9,58 dB), and the obtained results showed higher SNR values than the ones of the back wall echoes on first category blocks, ranging from 21,5 dB to almost 27,5 dB, (which was expected due to the decrease of scattering effect as already explained), while maintaining the slight descending tendency of SNR values over temperature, as seen in the previous tests (for the same reasons). Therefore, the results were more than sufficient to state that the equipment could clearly detect thickness discontinuities of 2 mm, from 30 mm to 12 mm steps, and temperatures between 25°C and 400°C.

Lastly, in order to better study the behaviour of different thickness discontinuities at 10 mm, A+C Scans of the third category block were analysed.

The results were treated using the same procedure as with previous blocks (Gain basis of 90 dB), therefore the charts regarding Amplitude vs. Temperature show the amplitude evolution along increasing temperatures described the same behaviour as with previous blocks (a descending tendency, with a slight slope decrease after around 200°C), for the same aforementioned reasons. But in this case, as geometric discontinuities created by the defects were not so accentuated when compared with first category blocks (the present blocks had Ø40 mm defects with depths of 2 mm, 3 mm and 4 mm), scattering due to this effect was reduced, therefore amplitude response was generally higher.

That also contributed to slightly higher SNR values from back wall echo in the SNR vs. Temperature charts. And generally, SNR values also followed the same tendency along increasing temperatures as the previous blocks, with noises around 10% and exhibiting SNR values well above the required minimum of 9,58 dB. Therefore, it was evident that the equipment could also detect thickness variations of 1 mm, from 2 mm depth to 4 mm depth, in 10 mm nominal thickness block, as it detected thickness variations on the previous second category block. As the required minimum of thickness discontinuities was 4 mm at a 10 mm block, it could be stated that the equipment satisfied the desired criterion.

On the ability to inspect tubular structures, it was tested and verified at the *Non Destructive Testing Laboratory* of *ISQ* that the scanner prototype could easily be coupled and removed to Carbon Steel pipes for circumferential and axial inspections.

Since the scanner prototype only weighted 3,1 Kg, and could easily be moved back and forth without much effort, it was comfortable enough to perform not only vertical inspections but also upside-down inspections.

During validation tests, scanning times were recorded using a chronometer, giving a mean value of 10 s which, with the scanning length (that was 210 mm, due to the Aluminium profiles on top of the heating box that assured the same starting and ending point at every test) were then used to compute the scanning speed, having a mean value of 21 mm/s. That also satisfied the minimum speed requirement of 15 mm/s.

As equipment calibration would always be performed on *Non Destructive Testing Laboratory* before each industrial inspection, on-site setup time, (which consisted in taking the equipment from the travelling case, making the necessary connections, couple the scanner in the desired structure and turn on *PowerBox H*) wouldn't take more than 6 minutes, as it was tested. Therefore, the desired maximum setup time of 10 minutes wasn't surpassed.

Using a proper harness, *PowerBox H* could be attached to the chest and the scanner could be transported by hand, revealing to be portable enough to be taken into spaces of difficult access.

3. Conclusion

In the present work, the design and creation of *EMAT Heat Inspection* prototype was achieved. Its validation in laboratorial environment showed that the equipment allows corrosion mapping in Carbon Steel structures up to 400°C.

The work was developed by *IST*, in collaboration with the *Non Destructive Testing Laboratory* of *ISQ Group*, with the intent to create a portable equipment which enabled the execution of specific corrosion mapping inspections over high temperature Carbon Steel structures on the Petrochemical Industry, in a rapid and efficient manner, thus reducing the setup and inspection times, avoiding plant shutdowns and preventing the occurrence of industrial disasters.

After proper validation tests were performed, the study of its respective results, mainly regarding signal amplitude behaviours on various kinds of defects and specimens at temperatures from 25°C to 400°C led to various conclusions. Remembering each customer requirement, the accomplishments were the following:

- Detect defects with minimum diameter of 16 mm and depth of 50% of the nominal specimen thickness (from 10 mm to 30 mm) up to 400°C.

The tests using first category blocks have stated that the prototype successfully detected defects of at least Ø16

mm, on nominal thicknesses ranging between 10 mm and 30 mm, and between 25 ºC and 400ºC. That kind of flaws was very similar to those of pitting corrosion defects [35], thus it can be concluded that the equipment can detect pitting corrosion flaws with the same characteristics.

- Detect thickness discontinuities of at least 4 mm depth in structures of 10 mm nominal thickness up to 400ºC.

Thickness measurement tests on the second and third category blocks concluded that the equipment not only detected depth discontinuities from 2 mm to 4 mm, in blocks of 10 mm nominal thickness, but also detected 2 mm thickness discontinuities in blocks with steps from 30 mm to 12 mm depth, between 25ºC and 400ºC, surpassing the desired requirement. That being said, evidently the equipment can be used to detect uniform corrosion or erosion corrosion defects, which usually led to thickness losses similar to those on the tested blocks [36].

- Perform circumferential and axial inspections on pipes with a minimum outer diameter of 350 mm.

As seen, the scanner was designed to perform circumferential and axial inspections on pipes tubular surfaces of minimum outer diameter of 331 mm and 104 mm respectively, and experiments on *Non Destructive Testing Laboratory* concluded the scanner can be easily coupled to pipes.

- Perform bottom, vertical and upside-down inspections.

All validation tests were bottom inspections, and laboratory experiments on various structures have also shown that the scanner, of 3,1 Kg, was easy to move and confortable enough to perform vertical and upside-down tests.

- The production site won't need to be shut down in order to perform the testing.

As it could inspect the desired Carbon Steel structures up to 400ºC, the production site wouldn't need to be shut down for the surfaces to cool and to perform the industrial tests.

- No more than 10 minutes of setup time.

Experiments on the *Non Destructive Testing laboratory* of *ISQ* concluded that the setup time was around 6 minutes.

- Minimum scanning speed of 15 mm/s.

According to experiments, the scanning speed was around 21 mm/s, which satisfied the required minimum.

- Generate Corrosion Mapping Reports (A-Scan and C-Scan).

The A+C Scans were the basis of this equipment's corrosion mapping reports, and were available to be consulted both in *PowerBox H* and in a desktop.

- The equipment must be portable enough to be taken to spaces of difficult access.

PowerBox H can be harnessed to the chest and the scanner prototype can be transported by hand, making the equipment suitable to perform inspections in spaces of difficult access.

Despite the natural attenuation effects of the signal along increasing temperatures due scattering caused by defect geometries, vibrational interactions between the travelling ultrasonic waves and the microstructures of Carbon Steel, and the different behaviour of cementite vibrational interactions with the ultrasonic waves after reaching its Curie Temperature, the developed prototype fulfilled all the customer requirements.

Its capacity to inspect, on the given conditions, flaws due to uniform corrosion and erosion corrosion, and defects of critical depth due to pitting corrosion, generating corrosion mapping reports at service temperatures up to 400ºC in a practical and reliable manner, was validated.

It was concluded that EMAT Heat Inspection prototype could be used to successfully inspect high temperature Carbon Steel structures of the aforementioned kind, for corrosion mapping. In fact, the equipment is the only one on the NDT market which is able to perform inspections on the given structures up to 400ºC, for corrosion mapping with lower setup times and rapid report generations.

Therefore, the developed engineering solution managed to resolve the imposed Industrial challenges, creating an equipment that can propel, in near future, a solid and competitive market offer on Corrosion Inspection Services at High Temperatures.

References

[1] M. R. Simmons, 'Report of offshore technology conference (OTC) presentation', 2008.

[2] Michael Baker Jr. Inc. to US Department of Transportation; Pipeline and Hazardous Materials Safety Administration; Office of Pipeline Safety; Integrity Management Program (under Delivery Order DTRS56-02-D-70036), 'Pipeline Corrosion - Final Report', 2008.

[3] The New York Times, 'Death Toll Up to 6 in Blast', *www.nytimes.com*. [Online]. Available: https://www.nytimes.com/1988/05/07/us/death-toll-up-to-6-in-blast.html. [Accessed: 15-Oct-2018].

[4] Linda Ashton - The Washington Post, '1 DEAD, 6 MISSING AS BLAST AT SHELL OIL REFINERY ROCKS LOUISIANA TOWN', *www.washingtonpost.com*. [Online]. Available: https://www.washingtonpost.com/archive/politics/1988/05/06/1-dead-6-missing-as-blast-at-shell-oil-refinery-rocks-louisiana-town/a8ddcf3a-047d-4bd9-b23c-90d88a85639d/?utm_term=.e268a421eff3. [Accessed: 15-Oct-2018].

[5] Ben Winslow & Jacob Hancock - Deseret News, 'Refinery explosion injures 4', *www.deseretnews.com*, 2009. [Online]. Available: https://www.deseretnews.com/article/705277112/Refinery-explosion-injures-4-homes-evacuated.html. [Accessed: 12-Oct-2018].

[6] CSB, 'CSB Releases Analysis Showing Cause of Rupture and Hydrogen Blast in 2009 Silver Eagle Refinery Accident in Woods Cross, Utah', *www.csb.gov*, 2014. [Online]. Available: https://www.csb.gov/-csb-releases-analysis-showing-cause-of-rupture-and-hydrogen-blast-in-2009-silver-eagle-refinery-accident-in-woods-cross-utah-pipe-walls-thinned-due-to-corrosion-that-went-uninspected-for-years-/. [Accessed: 12-Oct-2018].

[7] Jeremy Miller - High Country News, 'The Bay Area Chevron explosion shows gaps in refinery safety', *www.hcn.org*, 2012. [Online]. Available: https://www.hcn.org/issues/44.15/the-recent-bay-area-chevron-explosion-shows-gaps-in-refinery-safety. [Accessed: 12-Oct-2018].

[8] Braden Reddall & Erwin Seba - Reuters, 'Chevron's California refinery fire contained, not out yet', *www.reuters.com*, 2012. [Online]. Available: https://www.reuters.com/article/us-refinery-fire-chevron-richmond/chevrons-california-refinery-fire-contained-not-out-yet-idUSBRE87602Y20120807. [Accessed: 15-Oct-2018].

[9] K. Elayaperumal and V. Raja, *Corrosion Failures - Theory, Case Studies and Solutions*. Wiley, 2015.

[10] A. McLay and J. Verkooijen, 'Ultrasonic inspections at elevated temperature', *18th World Conf. Nondestruct. Test.*, vol. 54, no. 6, pp. 307–309, 2012.

[11] 'Standard Guide for Corrosion-Related Failure Analysis (ASTM Designation G161-00)', *Annu. B. ASTM Stand.*, vol. 00, no. Reapproved 2013, pp. 1–5, 2005.

[12] M. Hirao and H. Ogi, *Electromagnetic Acoustic Transducers - Noncontacting Ultrasonic Measurements using EMATs*, Springer. 2004.

[13] American Society for Testing and Materials (ASTM), 'Standard Guide for Electromagnetic Acoustic Transducers (EMATs) (Designation: E 1774 - 96)', vol. 03, no. Reapproved, pp. 1–8, 2002.

[14] R. Ribichini, F. Cegla, P. B. Nagy, and P. Cawley, 'Evaluation of electromagnetic acoustic transducer performance on steel materials', *NDT&E Int. 45 32–38*, vol. 1335, no. 1, pp. 785–792, 2011.

[15] R. B. Thompson, 'Electromagnetic Acoustic Transducers (EMATs)', in *The Evaluation of Materials and Structures by Quantitative Ultrasonics*, Springer, Ed. Vienna: J. D. Achenbach, 1993.

[16] G. Hayward *et al.*, *Ultrasonic Measurement Methods*, vol. XIX. Academic Press, 1990.

[17] J. C. Duke Jr, *Acousto - Ultrasonics: Theory and Application*. Springer, 1988.

[18] F. Pinto, J. Barata, and P. Barros, *Ensaios Não Destrutivos*. ISQ, 1992.

[19] B. Raj, T. Jayakumar, and M. Thavasimuthu, *Practical Non-Destructive Testing*. Woodhead Publishing Ltd., 2002.

[20] C. Meola, S. Boccardi, and G. M. Carlomagno, *Nondestructive Evaluation*. 2017.

[21] Innerpsec, 'Standard Sensors & Accessories for EMAT Applications'. pp. 1–209, 2017.

[22] K. Lee and T. Nelligan, 'The use of magnetostrictive EMAT transducers on oxide scaled boiler tubes', *16th WCNDT 2004 - World Conf. NDT*, pp. 1–5, 2004.

[23] M. I. Afandi, H. Adinanta, A. Setiono, Qomaruddin, and B. Widiyatmoko, 'High resolution extensometer based on optical encoder for measurement of small landslide displacements', *J. Phys. Conf. Ser.*, vol. 985, no. 1, pp. 0–6, 2018.

[24] 'Morgan Advanced Materials - Data sheet Superwool Boards', 2017.

[25] IAEA, *Non-destructive Testing: A Guidebook for Industrial Management and Quality Control Personnel*, no. 9. Vienna, 1999.

[26] ISQ, 'ISQ Group Technical Procedure (Internal Report)'. 2019.

[27] N. Lunn, S. Dixon, and M. D. G. Potter, 'High temperature EMAT design for scanning or fixed point operation on magnetite coated steel', *NDT E Int.*, vol. 89, no. October 2016, pp. 74–80, 2017.

[28] G. S. Darbari, R. P. Singh, and G. S. Verma, 'Ultrasonic attenuation in carbon steel and stainless steel at elevated temperatures', *J. Appl. Phys.*, vol. 39, no. 5, pp. 2238–2245, 1968.

[29] E. Papadakis, 'Ultrasonic Attenuation in Hot Specimens by the Momentary Contact Method with Pressure Coupling', *J. Acoust. Soc. Am.*, vol. 50, no. 1A, pp. 115–115, 2005.

[30] P. Edmonds, *Methods of Experimental Physics Vol. 19 - Ultrasonics*. Academic Press, 1981.

[31] T. Wan, T. Naoe, T. Wakui, M. Futakawa, H. Obayashi, and T. Sasa, 'Effects of Grain Size on Ultrasonic Attenuation in Type 316L Stainless Steel', *MDPI Mater. J.*, vol. 10, no. 7, p. 17, 2017.

[32] R. C. Tripathi and G. S. Verma, 'Ultrasonic attenuation as function of temperature in a 1% carbon steel', *J. Acoust. Soc. Am.*, vol. 53, no. 5, pp. 1344–1345, 2005.

[33] W. D. Callister and J. Wiley, 'Materials Science: an Introduction', p. 990, 2014.

[34] L. Mauger *et al.*, 'Phonons and elasticity of cementite through the Curie temperature', *Phys. Rev. B*, vol. 95, no. 2, pp. 1–9, 2017.

[35] M. Baker, 'Pipeline Corrosion Report', no. November, pp. 1–78, 2008.

[36] E. McCafferty, *Introduction to Corrosion Science*. Springer, 2010.